NJC

Accepted Manuscript

This is an *Accepted Manuscript*, which has been through the Royal Society of Chemistry peer review process and has been accepted for publication.

Accepted Manuscripts are published online shortly after acceptance, before technical editing, formatting and proof reading. Using this free service, authors can make their results available to the community, in citable form, before we publish the edited article. We will replace this *Accepted Manuscript* with the edited and formatted *Advance Article* as soon as it is available.

You can find more information about *Accepted Manuscripts* in the Information for Authors.

Please note that technical editing may introduce minor changes to the text and/or graphics, which may alter content. The journal's standard Terms & Conditions and the Ethical guidelines still apply. In no event shall the Royal Society of Chemistry be held responsible for any errors or omissions in this *Accepted Manuscript* or any consequences arising from the use of any information it contains.

ROYAL SOCIETY OF CHEMISTRY

www.rsc.org/njc

RSCPublishing

LETTER

Cite this: DOI: 10.1039/xoxxoooooox

Study of photocatalytic properties of bio-mimicked hollow SnO_2 microstructures synthesized with *Ceiba pentandra* (L.) Gaertn. (kapok) as a natural template †

Received ooth January 2014,
Accepted ooth January 2014

DOI: 10.1039/xoxxoooooox

www.rsc.org/

Young Jin Kim[1,a], Xing Xing[1,b], Do-Young Choi[c], Cheol-Ho Hwang[d], Chulmin Choi[e], Gunwoo Kim[a], Sungho Jin[a,e], Kyung-Jun Hwang[*,e], and Ju-Young Park[*,f]

Hollow SnO_2 microstructures (HSM) with mesoporous surface have been simply fabricated by template impregnation technique using *Ceiba pentandra* (L.) Gaertn. (kapok) as a natural template. The HSM could be used as an efficient photocatalyst for methylene blue dye photodegradation.

Effective design and control over the morphology and the functional properties of metal oxide microstructures have been a long-terms project in the development of chemical fabrication processes.[1] In the past few decades, tin oxide (SnO_2) has been widely applied in the fields of gas sensors,[2] secondary batteries,[3] light-emitting diodes,[4] photovoltaics,[5] water splitting, and photo-catalyst[6] due to its excellent electrical, optical, and photochemical properties. These properties are usually dependent on SnO_2 microstructures. Thus, a great deal of effort has been made by many researchers on synthesis of various SnO_2 microstructures such as spherical,[7] cubic,[8] wire,[9] rod,[10] fiber,[11] hollow spheres,[12] etc. In general, SnO_2 microstructures have been controlled by chemical reaction such as sol-gel, hydrothermal, and sonochemical method.[13] Although the synthetic technique has been improved steadily, controlling and modifying the microstructures of SnO_2 are still challenging. Each distinctively shaped SnO_2 particles stated above exhibits unique properties compared to the bulk state of SnO_2.[14] Hollow structures in particular have attracted the attention of researchers because they have many advantages over other shapes, including a large surface area, effective light scattering, and low density.[15] Recently, various methods have been used to fabricate hollow SnO_2 microstructures (HSM) through the soft or polymer template approach,[16] the emulsion method, and electro-spun method.[17] Among the various methods that are utilized in HSM preparation, the template approach is a scalable synthetic method for the mass production.[18] Recycling abundant natural material as raw template also produces ecological benefits. Among the various bio-resources available, the seeds of the kapok (*Ceiba pentandra* (L.) Gaertn.) tree are well-known as a hollow fiber resource that is widely available throughout Southeast Asia, Africa, and the South America.[19] Currently, various efforts have been made to develop high-performance photo-catalysts for the degradation of organic pollutants such as dyestuff and volatile organic compound (VOC) in water and air purification.[20] In the past few decades, many photocatalytic materials such as TiO_2 and ZnO which absorb a limited range of ultraviolet (UV) rather than a wider spectrum, have been the focus of research that has been conducted at great length.[21] Recently, the limitation has been overcome by hybrid photocatalysts such as composite photocatalyst ($ZnO/TiO_2/SnO_2$, ZnO/SnO_2, and SnO_2/TiO_2) and metal or organic element doped photocatalyst (Ag-TiO_2, N-TiO_2, Fe-TiO_2, and Sn-TiO_2). These have been widely examined due to their high photocatalytic properties, anti-recombination between electron (e^-) and hole (h^+) pair, and wider light absorbance spectrum which include visible light.[22] However, the systematic photocatalyic study of SnO_2 is not adequately done yet. In this work, we have focused on hollow SnO_2 microstructures, which were fabricated by template impregnation technique using kapok as a bioresource template, to investigate their properties for a potential photocatalyst in the photodegradation of methylene blue (MB).

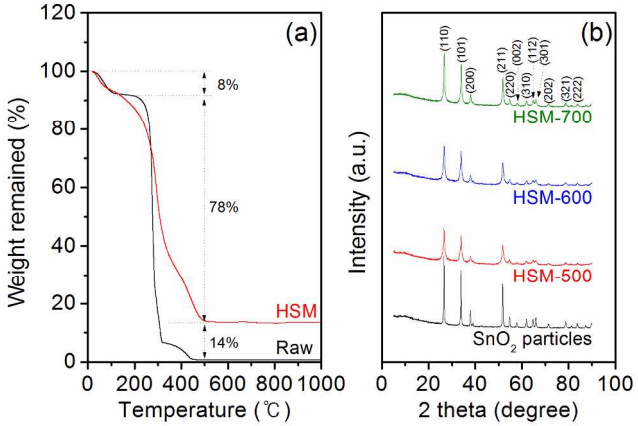

Fig. 1. (a) Thermal gravity analysis of raw kapok fiber (raw) and precursor as tin chloride immersed on kapok fiber (HSM); (b) X-ray diffraction patterns of hollow SnO_2 microstructure synthesized on kapok fiber template depending on calcination temperature. HSM-500, 600, and 700 are calcinated at 500 °C, 600 °C, and 700 °C respectively. The SnO_2 particles synthesised by template impregnation are compared to the SnO_2 particle synthesized by a conventional sol-gel process.

According to the referenced research,[23, 24] the hydroxyl and ether groups in natural cellulose can easily combine with SnO_2 synthetic precursor such as $SnCl_2$, leading to the intermediate formation of tin alkoxide groups, which can poly-condense with tin chloride groups to give thin oxo bridges as below (Eq. 1~3):

$$\text{Sn-Cl} + \text{ROH} \rightarrow \text{Sn-OR} + \text{HCl} \quad \text{(Eq. 1)}$$
$$\text{Sn-Cl} + \text{ROH} \rightarrow \text{Sn-OR} + \text{RCl} \quad \text{(Eq. 2)}$$
$$\text{Sn-Cl} + \text{Sn-OR} \rightarrow \text{Sn-O-Sn} + \text{RCl} \quad \text{(Eq. 3)}$$

This reaction pathway is quite efficient route for replication of tin oxide from nature template because kapok is mainly composed of cellulose fibers.[25] **Fig. 1(a)** shows the plots of the thermo-gravimetric analysis of the raw kapok fibers and the $SnCl_2$ precursor immersed kapok fibers. In the first plot for raw kapok fibers, the first weight loss of about 8% is due to moisture reduction. In the second weight loss step, which shows steep decrease, is related to decomposition of the organic compound such as cellulose and lignin of kapok fiber.[26] The kapok fibers completely decomposed at about 500 °C. Meanwhile, in the plot for $SnCl_2$ precursor immersed kapok templates, the first weight loss about 8% is due to the loss of moisture and volatile compounds. The 78% decrease of weight shown in the second step is due to the conversion of SnCl → SnO_2 by thermal-decomposition of the kapok fiber and crystallization.[27] Finally, the kapok fibers completely burnt out, and only SnO_2 was left. The yield of obtained HSM above 500 °C was about 14%. The X-ray diffraction analysis was used to study the crystallinity and crystallite size of the HSM samples. **Fig. 1(b)** shows the XRD patterns of the HSM samples synthesized on kapok fiber template, depending on calcination temperature.

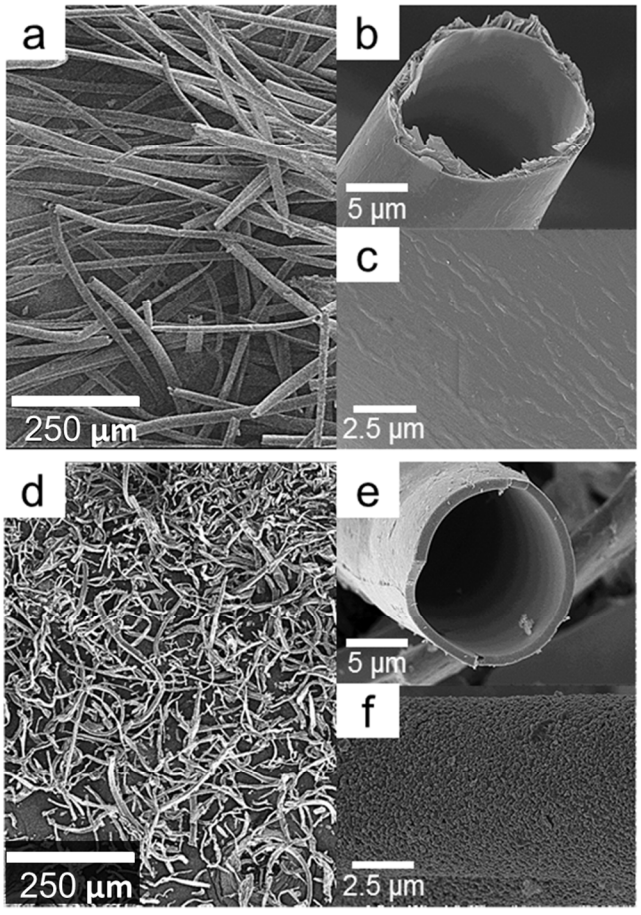

Fig. 2. Field emission-scanning electron microscopy images of raw kapok fiber (above pictures) and HSM (below pictures) after calcination at 600 °C: (a and d) low resolution shape images; (b and e) cross-sectional images; (c and f) high resolution surface images.

The sharp intense peak at the Bragg 2θ theta angle of 26.7° is the representative for the tetragonal phase deflection in all the samples. The XRD patterns of the samples matched well with the standard tetragonal SnO_2 pattern (d_{110}, d_{101}, d_{200}, d_{211}, d_{220}, d_{002}, d_{310}, d_{112}, and d_{301}; JCPDS Card No.00-041-1445). The widened peaks indicate that the particles are nano-sized and the samples have defects. The size of crystallite varies from 14.1 nm to 22.7 nm depending on the calcination temperatures. The average crystallite size increases as the calcination temperature increases. Also, all crystallite size of HSM is smaller than that of SnO_2 particles which has crystallite size of 31.4 nm. The average crystalline size was calculated using Sherrer's equation at corresponding angle (2θ =26.7°).[28]

Fig. 2(a and d) shows the low resolution overall image of raw kapok fiber as template material and the image of HSM using FE-SEM after calcination. The cross-sectional fiber images in Fig. 2(b and e) show that both hollow structures have an average diameter of 15 µm and an average thickness of 1 µm. After the calcination process, the HSM maintains the unique fiber structures of the original kapok template. **In the Fig. 2(c and f)**, the surface morphologies of kapok template and HSM materials were investigated in high-resolution mode. The HSM surface shows that the SnO_2 nanostructure formation and crystallinity growth have taken place after calcination and the SnO_2 nano particles are interconnected with nano-sized pores. On the contrary, the raw kapok template has a smooth surface without micro-pores.

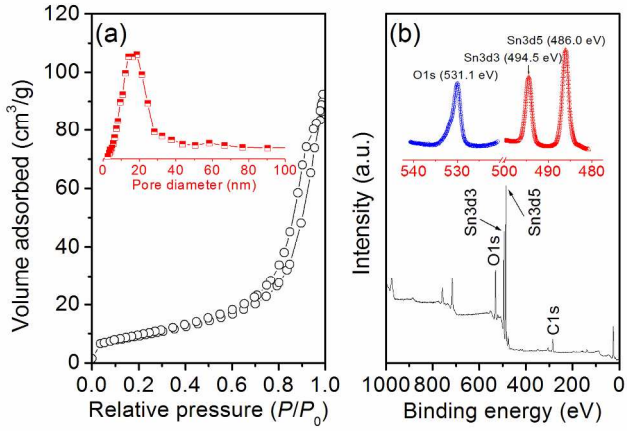

Fig. 3. (a) N_2 gas adsorption-desorption isotherms and pore-size distribution curve, (b) X-ray photoelectron spectra survey data, Sn 3d core level, and O 1s core level of HSM after calcination at 600 °C.

Fig. 3(a) show adsorption-desorption isotherms and pore size distribution curve of N_2 gas at 77 K for HSM samples after calcination at 600 °C. It illustrates the shape and behaviour of the N_2 adsorption isotherms for nano-porous materials. The isotherm curve shape is similar to type IV in the IUPAC classification[29] Herein, the type IV isotherm curve is wide, no clear plateau is attained, and a weakly hysteresis slope can be observed at intermediate and high relative pressures in HSM, which is indicative of the presence of nano-pores. The IV isotherm curve also indicates distributions of particle size between 5 and 40 nm. The adsorption and desorption isotherms line for HSM overlapped completely in the low relative pressure range (P/P_0=0.0~0.4), while the hysteresis loop was in the high relative pressure region ($P/P_0 > 0.4$), mainly due to the presence of ink-bottle shaped mesopores which is classified under IUPAC

pore size classification.[30] These ink-bottle type pore have a larger pore size in the bottle body, which induces hysteresis in the high relative pressure region. The specific surface area and average pore-size of HSM sample was found to be 53.1 m^2/g and 18.5 nm, using Brunauer-Emmett-Teller (BET) and Barrett-Joyner-Halenda (BJH), respectively.[31] For reference, the specific surface area of sol-gel produced SnO_2 particles used in this work is 4.3 m^2/g. The chemical composition of the HSM materials after calcination at 600 °C was also studied by XPS analysis on the **Fig. 3(b)**. The fully scanned survey spectra demonstrate that Sn, O, and C elements exist in HSM. The C element can be ascribed to the adventitious carbon-based contaminant from the kapok fiber after calcination, and the binding energy for the C 1s peak at 283.5 eV is used as the reference for calibration. The high resolution XPS spectra (Sn 3d and O 1s core-level) scanning over the following areas are analyzed: the binding energies for the the Sn 3d region around 490 eV, and the O 1s region around 531.1 eV. As shown in inside figure, there are two main peaks in the Sn 3d region. The peak located at 494.5 eV corresponds to the Sn $3d_{3/2}$ and another one located at 486.0 eV is assigned to Sn $3d_{5/2}$. The splitting of Sn 3d doublet of Sn between Sn is 8.5 eV, indicating that the valence state on Sn is +4.[32] Moreover, there are the O 1s photoelectron peaks. The shape of a sharp and symmetric peak of O 1s spectrum indicates that there can be one chemical state according to the binding energy. It mainly includes crystal lattice oxygen (O_{Sn-O}) and a small amount of surface hydroxyl groups (O_{OH}) and adsorbed water with increasing binding energy. Using the XPS Peak fitting program, the contents of Sn and O of HSM materials were calculated 26.3% and 53.79% corresponding closely SnO_2 stoichiometry. Generally, similar results are observed in SnO_2 porous materials.[33]

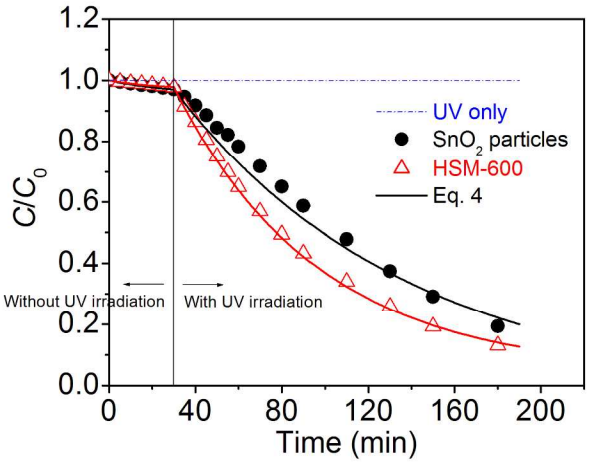

Fig. 4. Methylene blue photo-decomposition curves of HSM calcinated at 600 °C and sol-gel produced SnO_2 particles under UV irradiation after adsorption reaction.

Fig. 4 shows the MB degradation curves by photo catalytic reaction of HSM calcinated at 600 °C and the sol-gel produced SnO_2 nanoparticles (see ESI† for MB photo-decomposition curves by HSM-500 and HSM-700). During the first 30 min, without UV irradiation, the decrease of MB concentration was mainly due to the adsorption of MB into the HSMs. [34] In this adsorption equilibrium stage, the initial concentration of MB was reduced about 3%. The adsorption kinetics of MB on HSMs and SnO_2 particles are very similar. As UV irradiation began at 30 min, the concentration of MB decrease swiftly due to the photocatalytic reaction of HSMs and SnO_2 particles. Consequently, the concentration of MB decreased by 90% and 80% by HSMs and sol-gel produced SnO_2 particles respectively. The photo-decomposed rate was faster in the case of HSM-600 (0.021 min^{-1}) than in the case of sol-gel produced SnO_2 particles (0.017 min^{-1}). This result is related with the high surface area of HSMs, which can consequently adsorb a large amount of MB, water, and oxygen molecules and then eventually decompose much of it on the surface of HSMs during a photocatalytic reaction. In this work, the photocatalytic decomposition is a pseudo-first order reaction, and its kinetics can be express by Langmuir–Hinshelwood (Eq. 4) as below:

$$ln\left(\frac{C_o}{C}\right) = -kKt = -k_{app}t \qquad \text{(Eq. 4)}$$

where, k_{app} is the apparent rate constant, and C_0 and C are the initial solution concentration and after degradation of MB solution, respectively. This apparent rate constant for degradation of dye was obtained by calculating the correlation between the length of time of UV light irradiation and the decreasing ratio of dye,[35] determined by using above Equation (4).[36]

In conclusion, hollow SnO_2 micro-structured materials were synthesized by a template impregnation technique using natural kapok fiber as sacrificial templates. This synthesis method is simple, scalable and highly coast effective compare to other fabrication method such as electrospinning, hydrothermal and sol-gel. The specific surface area of the SnO_2 synthesized using sacrificial Kapok fiber was three times larger than the nano-sized SnO_2 particles that are produced by conventional sol-gel method. The result shows the HSM particles that were calcinated at 500 °C also have a tetragonal phase. The structure of the nature templates was well replicated on the HSMs, and the high surface area improved the efficiency of the photocatalytic reaction. Under the irradiation of ultra violet light, methylene blue was degraded from dye percent of 100% to 10% in 200 min. In summary, the hollow SnO_2 microstructure could be offered a new photocatalyst for removal organic dyes in wastewater.

Experimental section

Kapok [*Ceiba pentandra* (L.) Gaertn.] fibers were obtained from Java Island, Indonesia. The kapok fibers were air-dried and subsequently oven-dried at 120 °C for 24 h to remove the moisture content. Anhydrous ethanol (Sigma-Aldrich, USA), distilled water, tin (II) chloride dehydrate (for SnO_2), all purchased from Sigma-Aldrich (USA), were analytical grade (assay > 99%) and used without further purification. In a typical synthesis, 0.1 M of the tin oxide (SnO_2) precursor was added into a beaker and dissolved in a solvent of anhydrous ethanol or distilled water. The impregnation reaction was then performed at 25 °C for 6 h. After the reaction, the SnO_2/kapok template was washed with anhydrous ethanol and dried in vacuum at 80 °C for 4 h. The samples were then calcinated at 500 to 700 °C for 4 h to remove the kapok templates and obtain hollow SnO_2 microstructures (HSM). Thermo gravimetric analysis (TGA; STARSW, Mettler-Toledo, USA) was conducted up to 1,000 °C with a heating rate of 2 °C/min under air atmosphere to evaluate the thermal behaviour of the HSM. The surface and shape of the HSM was investigated by field emission scanning electron microscopy (FE-SEM; S-4700, Hitachi, Japan). The surface area and pore volume of the prepared HSMs were measured by using a nitrogen adsorption and desorption analyzer (BET; ASAP 2020, Micromeritics, USA) after preheating the samples to 200 °C for 2 h to eliminate surface contaminants, including adsorbed water. The pore size distributions were obtained by applying the Barrett-Joyner-Halenda (BJH) equation to the nitrogen adsorption isotherms at -169.15 °C. The X-ray diffraction (XRD) patterns were obtained on a D/MAX-2500 (Rigaku, Japan) using Cu-Kα radiation (λ = 1.540 Å). The X-ray photoelectron spectra (XPS) were collected on a Surface Science SSX100 (Seal Laboratories, USA) using Mg-Kα X-rays as the excitation source. The absorption spectra of the samples

in 190-900 nm wavelength range was measured using a double-beam UV-visible spectrophotometer (UV-210, Shimadzu). The photocatalytic degradation of a methylene blue solution was performed by placing a 500 mL quartz tube in the middle of four 4 W UV lamps (30 cm length × 2.0 cm diameter; Philips, USA). The lamps were positioned inside a cylindrical Pyrex vessel, and cooled by a circulating water column to remove heat. The UV irradiation power flux of the reactor was 1.84 mW/cm^2. 0.3 g of photocatalyst (HSM; 0.3 g) and 500 mL of methylene blue (MB) solution (10.0 mg L^{-1}) were put into the quartz tube. During the first 30 minutes the solution was stirred without UV irradiation to establish an adsorption equilibrium condition. UV irradiation began after the 30 min. The initial concentration of MB (C_0) and the change of concentration during photodecomposition (C) were determined using a UV-Vis spectrometer at 660 nm. 5 ml of the solution was pumped into a cuvette in the UV-Vis spectrometer every 10 minute for the measurement, and pumped back to the photodegradation apparatus using computer controlled syringe pump. The apparatus was kept in darkness all the time (see ESI† for the schematics of the photodegradation apparatus).

Acknowledgements

This research was supported by Basic Science Research Program through the National Research Foundation of Korea (NRF) funded by the Ministry of Education (NRF-2013R1A6A3A03021144).

Notes and references

[a]*Materials science and Engineering, University of California at San Diego, La Jolla CA 92093, USA. E-mail: yjk019@ucsd.edu (Y. Kim)*
[b]*Department of Nanoengineering, University of California at San Diego, La Jolla CA 92093, USA. E-mail: x1xing@eng.ucsd.edu (X. Xing).*
[c]*KHT Engineering Co., ltd., Gunpo-si 435-833, South Korea. E-mail: tenstone@hanmail.net (D.-Y. Choi).*
[d]*International Climate and Environment Center, Gwangju 502-861, South Korea. E-mail: cheolhoh@hanmail.net (C.-H. Hwang).*
[e]*Mechanical and Aerospace Engineering, University of California at San Diego, La Jolla CA 92093, USA. E-mail: kyhwang@ucsd.edu (K.-J. Hwang); cnchoi@eng.ucsd.edu (C. Choi); gunwoo@ucsd.edu (G. Kim); sjin@ucsd.edu (S. Jin).*
[f]*Green Energy Institute, Mokpo-Si 530-400, Republic of Korea. E-mail: juyoungpark@gei.re.kr (J.-Y. Park).*
[1]*These authors contributed equally to this work.*

1. Q. Zhang, H.-Y. Wang, X. Jia, B. Liu and Y. Yang, *Nanoscale*, 2013, **5**, 7175.
2. W. Zeng, T. Liua and Z. Wang, *Journal of Materials Chemistry*, 2012, **8**, 3544.
3. Q. Guo, Z. Zheng, H. Gao, J. Ma, X. Qin, *Journal of Power Sources*, 2013, **15**, 149.
4. Y. Li, W. Yin, R. Deng, R. Chen, J. Chen, Q. Yan, B. Yao, H. Sun, S.-H. Wei, T. Wu, *NPG Asia Materials*, 2012, **4**, e30.
5. Asdim, K. Manseki, T. Sugiura and T. Yoshida, *New J. Chem.*, 2014, **38**, 598.
6. R. Saito, Y. Misekia and K. Sayama, *Chemical Communications*, 2012, **48**, 3833.
7. T. Kida, S. Fujiyama, K. Suematsu, M. Yuasa, K. Shimanoe, *Journal of Physical Chemistry C*, 2013, **117**, 17574.
8. R.Liu, S.Yang, F. Wang, X. Lu, Z. Yang, B. Ding, *ACS Applied Materials & Interfaces*, 2012, **4**, 1537.
9. C. Nam, D. Hong, J. Chung, J. Chung, I. Hwang, J. Lee, S. Ko, C. P. Grigoropoulos, *Japanese Journal of Applied Physics*, 2010, **49**, 05EA12.
10. V. Ganapathy, E.-H. Kong, Y.-C. Park, H. M. Jang, S-W. Rhee, 2014, **6**, 3296.
11. J. Shin, S.-J. Choi, I. Lee, D.-Y. Youn, C. O. Park, J.-H. Lee, H. L. Tuller, I.-D. Kim, *Advanced Functional Materials*, 2013, **23**, 2357.
12. S. Ding, J. S. Chen, G. Qi, X. Duan, Z. Wang, E. P. Giannelis, L. A. Archer, X. W. Lou, *Journal of American Chemical. Society*, 2011, **133**, 21.
13. M. Aziz, S. S. Abba and W. R. W. Baharom, *Materials Letters*, 2013, **91**, 31.
14. X. Wang, Z. Li, Q. Li, C. Wang, A. Chen, Z. Zhang, R. Fan and L. Yin, *CrystEngComm*, 2013, **15**, 3696.
15. F. Zhang, K.-X. Wang, X.-Y. Wang, G.-D. Li, J.-S. Chen, *Dalton Transactions*, 2011, **40**, 8517.
16. Y. Yin, S. Xin, L. Wan, C. Li, Y. Guo, *Science China Chemistry*, 2012, **55**, 1314.
17. R. A. Kadir, Z. Li, A. Z. Sadek, R. A. Rani, A. S. Zoolfakar, M. R. Field, J. Z. Ou, A. F. Chrimes, K. Kalantar-zadeh, *Journal of Photochemistry and Photobiology C,* 2014, **118**, 3129.
18. T. T. Vu and G. Marbán, *Applied Catalysis B: Environmental,* 2014, **25**, 51.
19. X. Zhang, C. Duan, N. Zhao, H. Xiao, M. Shi, X. Zhang, J. Xu, *Chinese Journal of Polymer Science*, 2010, **28**, 841.
20. L. Zoua, Y. Luo, M. Hooper, E. Hu, *Chemical Engineering and Processing*, 2006, **45**, 959.
21. S. Anandan, N. Ohashi and M. Miyauchi, *Applied Catalysis B: Environmental*, 2010, **100**, 502.
22. C. Di Valentin, E. Finazzi, G. Pacchioni, A. Selloni, S. Livraghi, M. C. Paganini, E. Giamello, *Chemical Physics*, 2007, **339**, 44.
23. B. Boury, R. G. Nair, S. K. Samdarshi, T. Makiabadi, P. H. Mutin, *New Journal of Chemistry*, 2012, **36**, 2196.
24. K. Bouras, J.-L. Rehspringer, G. Schmerber, H. Rinnert, S. Colis, G. Ferblantier, M. Balestrieri, D. Ihiawakrim, A. Dinia and A. Slaoui, *J. Mater. Chem. C*, 2014, **2**, 8235.
25. Y. K. Walia, K. Kishore, D. Vasu, D. K. Gupta, *International Journal of Theoretical & Applied Sciences*, 2009, **1**, 15.
26. S. Draman, R. Daik, F. Latif, S. M. El-Sheikh, *Bioreseources*, 2014, **9**, 8.
27. J. W. Ko, B. I. Lee, Y. J. Chung and C. B. Park, *Green Chem.*, 2015, DOI: 10.1039/C5GC01348H.
28. B. D. Cullity and S. R. Stock, *Elements of X-ray diffraction*. 3rd ed. New Jersey: Prentice Hall, 2011.
29. A. Morsli, A. Benhamou, J.-P. Basly, M. Baudu and Z. Derriche, *RSC Adv.*, 2015, **5**, 41631.
30. M. Thommes, B. Smarsly, M. Groenewolt, P. I. Ravikovitch, A. V. Neimark, *Langmuir*, 2006, **22**, 756.
31. W. Wang, T. Jiao, Q. Zhang, X. Luo, J. Hu, Y. Chen, Q. Peng, X. Yan and B. Li, *RSC Adv.*, 2015, **5**, 56279-56285.
32. M. Kwokaa, L. Ottaviano, M. Passacantando, S. Santucci, G. Czempik, J. Szuber, *Thin Solid Films*, 2005, **490**, 36.
33. L. L. Li, W. M. Zhang, Q. Yuan, Z. X. Li, C. J. Fang, L. D. Sun, L. J. Wan, C. H. Yan, *Crystal Growth & Design*, 2008, **8**, 4165.
34. K.-J. Hwang, J.-W. Lee, W.-G. Shim, H. D. Jang, S.-I. Lee, S.-J. Yoo, *Adv. Powder Tech.*, 2012, **23**, 414.
35. L. Zhang, H. Li, Y. Liu, Z. Tian, B. Yang, Z. Sun and S. Yan, *RSC Adv.*, 2014, **4**, 48703.
36. N. Tsuchiya, K. Kuwabara, A. Hidaka, K. Oda and K. Katayama, *Phys. Chem. Chem. Phys.*, 2012, **14**, 4734.

Table of Contents

Study of photocatalytic properties of bio-mimicked hollow SnO_2 microstructures synthesized with *Ceiba pentandra* (L.) Gaertn. (kapok) as a natural template

Young Jin Kim, Xing Xing, Chulmin Choi, Gunwoo Kim, Sungho Jin, Kyung-Jun Hwang, and Ju-Young Park

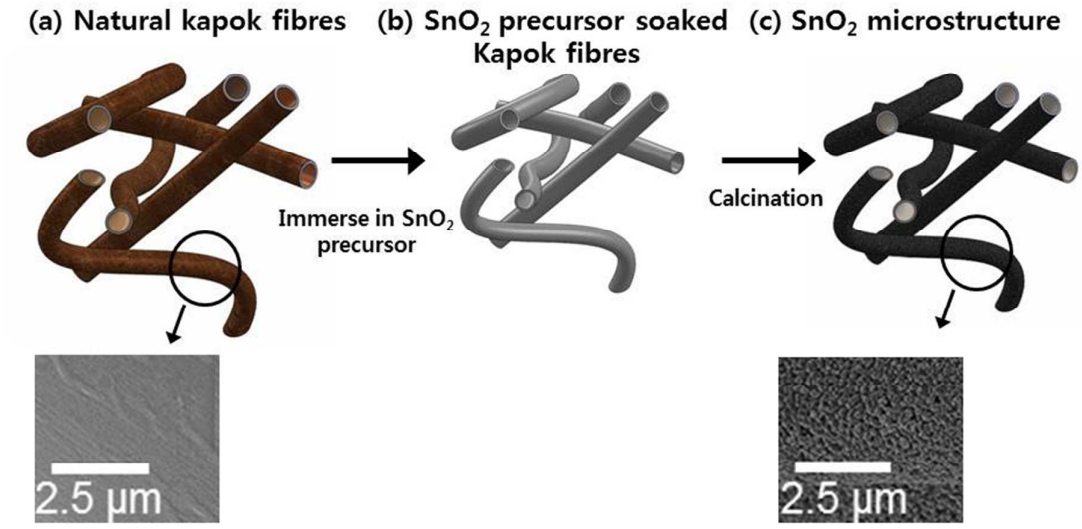

Hollow SnO_2 microstructures have been simply fabricated by template impregnation technique using *Ceiba pentandra* (l.) Gaertn. as a natural template.